

RSC Advances



This is an *Accepted Manuscript*, which has been through the Royal Society of Chemistry peer review process and has been accepted for publication.

Accepted Manuscripts are published online shortly after acceptance, before technical editing, formatting and proof reading. Using this free service, authors can make their results available to the community, in citable form, before we publish the edited article. This *Accepted Manuscript* will be replaced by the edited, formatted and paginated article as soon as this is available.

You can find more information about *Accepted Manuscripts* in the [Information for Authors](#).

Please note that technical editing may introduce minor changes to the text and/or graphics, which may alter content. The journal's standard [Terms & Conditions](#) and the [Ethical guidelines](#) still apply. In no event shall the Royal Society of Chemistry be held responsible for any errors or omissions in this *Accepted Manuscript* or any consequences arising from the use of any information it contains.

**Synthesis of amidoximated graphene oxide nanoribbons
from unzipping of multiwalled carbon nanotubes
for selective separation of uranium(VI)**

**Yun Wang ^{a,b}, Zhengshang Wang ^a, Ran Ang ^a, Jijun Yang ^a, Ning Liu ^{a,*},
Jiali Liao ^a, Yuanyou Yang ^a, and Jun Tang ^{a,*}**

*^a Key Laboratory of Radiation Physics and Technology, Ministry of Education,
Institute of Nuclear Science and Technology, Sichuan University, Chengdu 610064,
China*

*^b School of Chemistry, Biological and Materials Science, East China Institute of
Technology, Nanchang 330013, Jiangxi, China*

*Author to whom correspondence should be addressed, Email: tangjun@scu.edu.cn.

Phone: +86-28-85416215. Fax: +86-28-85416215

*Author to whom correspondence should be addressed, Email: nliu720@scu.edu.cn

Phone: +86-28-85416858. Fax: +86-28-85412374

Abstract

A kind of uranium-selective sorbent has been studied using graphene oxide nanoribbons (GONRs) from unzipping of multiwalled carbon nanotubes as solid matrix and amidoxime (AO) as functional group. Amidoxime-functionalized GONRs (AOGONRs) were successfully prepared by chemical grafting technology as characterized by scanning electron microscopy, X-ray power diffraction, fourier transformed infrared spectroscopy, elemental analysis, thermogravimetric analysis and X-ray photoelectron spectroscopy. The as-prepared AOGONRs were applied to adsorb U(VI) from aqueous solutions and exhibited a high sorption capacity towards U(VI) due to the strong chelation of AO to U(VI). It can be noted that uranium sorption on AOGONRs was pH-dependent, ionic strength-independent, fast, endothermic, spontaneous and a pseudo-second order process. The U(VI) sorption amount reached up to $2.112 \text{ mmol g}^{-1}$ (502.6 mg g^{-1}) at $\text{pH} = 4.5$ and $T = 298 \text{ K}$. The sorption study performed in a stimulated nuclear industry effluent demonstrated that the new sorbent had a desirable selectivity for U(VI) ions over a range of competing metal ions. The results suggest that AOGONRs may be a potential and suitable candidate for separation of U(VI) from various uranium-containing water.

Keywords: Graphene oxide nanoribbons, Amidoxime, Uranium(VI), Sorption

Introduction

Graphene,¹ a 2D single atomic layer of sp^2 carbon, has been regarded as a star material owing to its unique physical and chemical properties such as high thermal conductivity, large surface area, and good thermal stability in comparison to conventional allotropes of carbon.²⁻⁴ In the past years, many interests have been attracted for graphene in environment science. In particular, graphene oxide (GO) with abundant oxygen-bearing groups on the surface are much more hydrophilic than graphene itself, and thus can efficiently capture metal ions through sharing an electron pair of the oxygen atom.⁵ GO has been proved to be non-toxic and biodegradable and the adsorption/desorption of metal ions could be easily performed, which makes it suitable to be applied in environmental science.⁶⁻⁹ However, the high cost of GO greatly limit its large-scale applications, and the sorption capacity of metal ions on GO needs to be further improved. Therefore, exploring an alternative graphene-based material with a higher sorption capacity and lower cost for sorption of metal ions is imperative.

Particularly, nanometer-wide ribbons of graphene, namely graphene nanoribbons (GNRs), is one of the most promising materials for this purpose. Several approaches have been developed to synthesize GNRs, such as lithographic patterning, sonochemical methods, chemical vapor deposition and unzipping of multiwalled carbon nanotubes (MWCNTs).^{10, 11} Among these methods, oxidative chemical unzipping of MWCNTs using sulfuric acid (H_2SO_4) and potassium permanganate ($KMnO_4$) developed by Tour's group offered a unique way for bulk production of GNRs.¹² Since the unzipping process is oxidative and similar to GO, these nanoribbons are termed graphene oxide nanoribbons (GONRs) and possess oxygen-containing functional groups such as $-C=O$, $-COOH$ and $-OH$ at the edges and surfaces. These functional groups are essential for capturing metal ions, and also facilitate the following functionalization process. This provides a promising sorbent to remove metal ions from aqueous solutions. However, to the best of our knowledge, few studies have been reported in environmental application for GONRs. Recently,

our group firstly used GONRs to remove uranium from wastewater and an impressive maximum sorption amount of 394.1 mg g⁻¹ was achieved.¹³ But GONRs still showed poor selectivity toward nuclides of interest, and the sorption capacity was not high enough. Therefore, further investigation to improve selectivity and loading capacity of GONRs to uranium is of great importance.

Amidoxime (AO) groups, one of the most effective chelating functional groups, have attracted special attention for the removal of uranium from various aqueous solutions because of their high selectivity and affinity for uranium.¹⁴⁻¹⁷ Carbon-based materials with AO groups have been widely used as the sorbent for the removal of uranyl ions.¹⁸⁻²³ For instance, amidoxime-grafted hydrothermal carbon showed uranium sorption capacities as high as 466 mg g⁻¹ and demonstrated stronger selectivity at acidic medium.²⁴ Amidoximated magnetite/graphene oxide composites were applied to adsorb uranium from aqueous solutions and found a maximum sorption capacity of 284.9 mg g⁻¹.²⁵ Our group grafted amidoxime group onto MWCNTs by using plasma techniques to selectively separate uranium from simulated nuclear industrial effluents, and an optimum sorption capacity of 145 mg g⁻¹ for U(VI) was obtained.²⁶ In this work, amidoximated GONRs (AOGONRs) were synthesized using GONRs as the solid matrix and DAMN as a precursor of AO group. Then, the behavior of the new sorbent AOGONRs for the removal of U(VI) from uranium-containing aqueous solutions was studied in detail. Moreover, the possible sorption mechanism of the sorption process was explored.

Experimental

Chemicals and reagents

MWCNTs were obtained from Chengdu Institute of Organic Chemistry of the Chinese Academy of Sciences.

Chemicals and reagents such as N,N-dimethylformamide (DMF), tetrahydrofuran (THF), 4-dimethylamipryidine (DMAP), ethanol, dichloromethane, K₂CO₃, NaOH, HNO₃, and hydroxylamine hydrochloride (NH₂OH·HCl) used in this research were

purchased from Chengdu Kelong Chemical Reagent Co., Ltd. (China). Diaminomaleonitrile (DAMN) and 1-(3-dimethylaminopropyl)-3-ethyl-carbodiimide hydrochloride (EDCI) were purchased from Energy Chemical Co., Ltd. (China). All metal oxides and nitrates were purchased from Aladdin Chemistry Co., Ltd. (China). All reagents were of AR grade and were used without further purification.

Preparation of GONRs

GONRs were fabricated by longitudinally unzipping of MWCNTs.¹² Typically, 1 g of MWCNTs was immersed in 150 mL of sulfuric acid (H₂SO₄, 98%) for 6 h at room temperature. Then, 500 wt% of KMnO₄ was added to the reaction mixture and stirred for 1 h at room temperature. The mixture was then heated to 55 °C for 30 min. The reaction temperature was then raised to 70 °C, and then cooled to room temperature. Thereafter the mixture was poured onto 400 mL of ice containing 5 mL of 30% H₂O₂ solution and then filtered through a PTFE membrane (5.0 μm). The residue was washed with deionized water, followed by centrifugation and dialysis process (10 K, MWCO, for one week or more time) to remove the inorganic acid and impurities. Finally, the mixture was filtered through PTFE membrane and the filtered product was dried in vacuum oven at 60 °C for 24 h. The prepared samples were denoted as GONRs.

Preparation of AOGONRs

The as-prepared GONRs (2.0 g) and EDCI (2.2 g) were dispersed into THF (60 mL). Then 2.0 g of DAMN and 0.12 g of DAMP were dissolved in 10 mL DMF and added into the reaction system. The mixture was sonicated for 1h to get a homogeneous colloidal suspension and then refluxed for 24 h with stirring to graft DAMN onto GONRs. After the condensation reaction was terminated, the resultant was filtrated and washed with ethanol and deionized water until the filtrate became colorless. Then the resulting solid (GONRs-DAMN) was washed by dichloromethane to remove DMF, finally washed with ethanol thoroughly and dried in a vacuum oven at 60 °C. GONRs-DAMN was then treated with 1.0 g K₂CO₃ and 1.5 g NH₂OH·HCl

in a 50/50 H₂O-C₂H₅OH solution (pH 8.5) for 10 h at 80 °C in a closed flask. Finally the mixture was filtrated, the residue was separated, rinsed and dried at 60 °C in vacuum overnight, and the final AOGONRs product was obtained. The schematic presentation of the synthesis process is shown in Fig. 1.

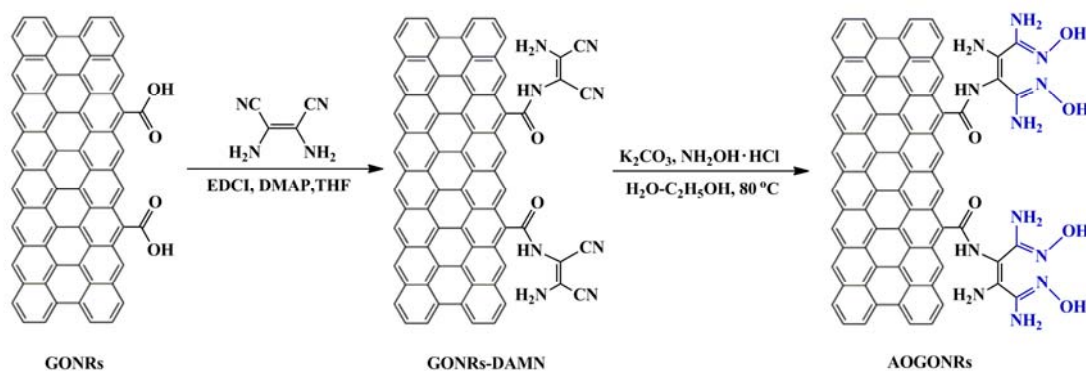


Fig. 1 Schematic illustration of the synthesis of AOGONRs.

Characterization

The samples were characterized by scanning electron microscopy (SEM), X-ray power diffraction (XRD), Fourier transformed infrared (FT-IR) spectroscopy, elemental analysis, thermogravimetric analysis (TGA) and X-ray photoelectron spectroscopy (XPS). The SEM images were performed on Hitachi S-4800 microscope. The XRD patterns were measured on a DX-2700 diffractometer with a Cu K α source. FT-IR spectra were obtained from Nicolet 6700 spectrometer. Contents of carbon, hydrogen, and nitrogen in samples were determined by elemental analyzer (Carlo-Erba 1106, Italy). TGA was carried out on TG 209 F1 in N₂ atmosphere from room temperature to 800 °C at a rate of 10 °C/min. The XPS spectra were recorded on Kratos AXIS ULTRA^{DL}D electron spectrometer with a multidetection analyzer using an Al K α X-ray source (1486.6 eV) at 10 kV and 5 mA under 10⁻⁸ Pa residual pressure.

Sorption experiments

Batch experiments were carried out to study the sorption behavior of AOGONRs to U(VI). A certain amount of sorbent was added into Erlenmeyer flasks with 25 mL

of either pure U(VI) solution or multi-ion solution (simulated nuclear industrial effluent sample) containing 12 co-existing cations (Table 1). Solution pH was adjusted using HNO₃ and NaOH solution and measured on a digital pH-meter. After being shaken for a specific time, the solutions were centrifuged at 9000 rpm for 30 min, and then the supernatant was filtered using 0.45 μm membrane filters. The initial and the residual concentration of uranium were determined by inductively coupled plasma optical emission spectroscopy (ICP-OES, Optima 8000, USA).

Table 1 Compositions of the simulated nuclear industrial effluent.

Coexistent ion	Added as	Reagent purity
UO ₂ ²⁺	UO ₂ (NO ₃) ₂ ·6H ₂ O	Standard reagent
La ³⁺	La(NO ₃) ₃ ·6H ₂ O	99.9% metal basis
Ce ³⁺	Ce(NO ₃) ₃ ·6H ₂ O	99.99% metal basis
Nd ³⁺	Nd(NO ₃) ₃ ·6H ₂ O	AR
Sm ³⁺	Sm(NO ₃) ₃ ·6H ₂ O	AR
Gd ³⁺	Gd(NO ₃) ₃ ·6H ₂ O	AR
Mn ²⁺	MnO	99.5%
Co ²⁺	Co(NO ₃) ₂ ·6H ₂ O	99.99% metal basis
Ni ²⁺	Ni(NO ₃) ₂ ·6H ₂ O	Spectrum pure
Zn ²⁺	Zn(NO ₃) ₂ ·6H ₂ O	99.99% metal basis
Sr ²⁺	Sr(NO ₃) ₂	99.99% metal basis
Ba ²⁺	Ba(NO ₃) ₂	99.999%

Sorption amount q_e (mmol g⁻¹) and distribution coefficient K_d (mL g⁻¹) were calculated by equation (1) and (2),

$$q_e = \frac{(C_0 - C_e) \times V}{w} \quad (1)$$

$$K_d = \frac{(C_0 - C_e) \times V}{C_e \times w} \quad (2)$$

where C_0 and C_e are the initial concentration and equilibrium concentration of metal ion (mmol L⁻¹), respectively. V is the volume of the testing solution (L), and w is the amount of sorbent (g).

Desorption and reusability studies

To carry out desorption experiment, the solid residue of sorption experiments was thoroughly rinsed with deionized water and dispersed in 25 mL HCl solution with different concentration, allowed to equilibrate for 2 h. After solid-liquid separation, the remaining U(VI) concentration in the supernatant was measured to evaluate the desorption percentage. To determine the reusability, consecutive sorption-desorption cycles were repeated for 5 times with the same sorbent using fresh U(VI) solution (0.25 mmol L^{-1} , pH = 4.5) at 298K. Regeneration of the sorbent was carried out using 0.5 mol/L HCl. All experimental series were performed at least in duplicates.

Results and discussion

Characterizations

The morphologies of MWCNTs, GONRs, GONRs-DAMN and AOGONRs were observed by SEM, as shown in Fig. 2. Pristine MWCNTs (Fig. 2a) are curved and entangled and have diameters ranging from 10-50 nm and lengths in the micrometer range. As can be seen in the Fig. 2b, MWCNTs were completely unzipped, resulting in complex, wavy-structured GONRs strips. The typical width of the strips lies in the 30-100 nm range, while the length of the strips lies in the micrometer range. The simple oxidative process can generate a nearly 100% yield of nanoribbon structures by lengthwise cutting and unraveling of the MWCNTs side walls.²⁷ Compared with GONRs, no obvious morphological changes were observed on the surfaces of functionalized GONRs (Fig. 2c-d), but they are more aggregated with each other, which may be attributed to the strong interaction between GONRs and functional groups such as AO.²⁸

Further structural information and the crystal plane of MWCNTs, GONRs, GONRs-DAMN and AOGONRs were characterized by XRD. As shown in Fig. 3, MWCNTs show a typical peak at $2\theta = 26.0^\circ$, corresponding to the interlayer space of 3.4 \AA , while GONRs show a predominant peak at $2\theta = 10.0^\circ$, corresponding to a

d-spacing of 8.6 Å. The result indicates the formation of GONRs from unzipping of MWCNTs.²⁹ However, in the XRD patterns of GONRs-DAMN and AOGONRs, the peak at $2\theta = 10.0^\circ$ disappears and a new peak also appears at 26.0° . The decrease in interplanar spacing indicates that the structure of GONRs has changed and the graphene layers of GONRs have been compacted after functionalization.³⁰ This change can be attributed to the grafted functional groups strengthening the interaction between GONRs,³¹ which was also confirmed by SEM.

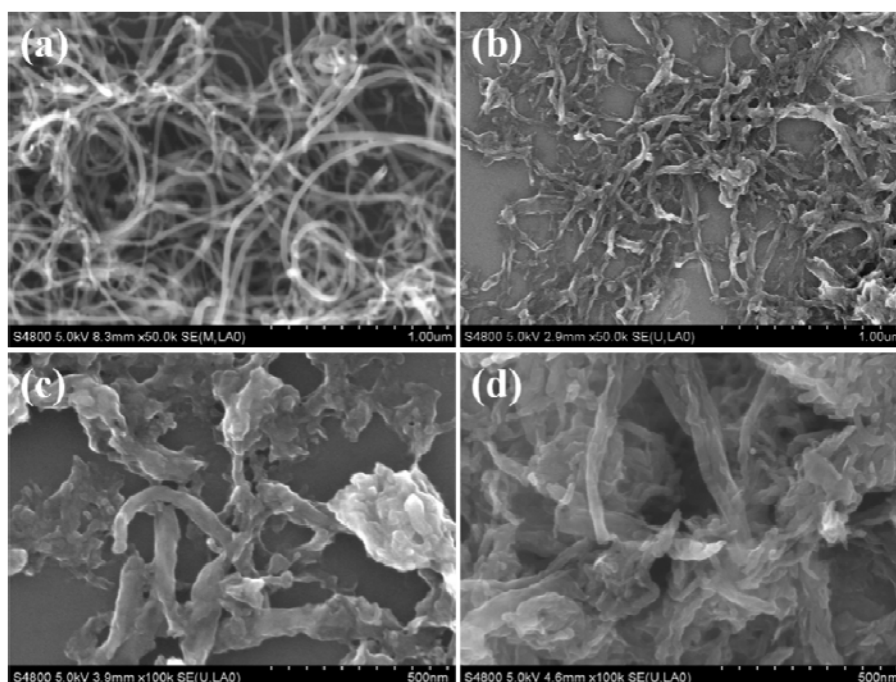


Fig. 2 SEM images of (a) MWCNTs, (b) GONRs, (c) GONRs-DAMN and (d) AOGONRs.

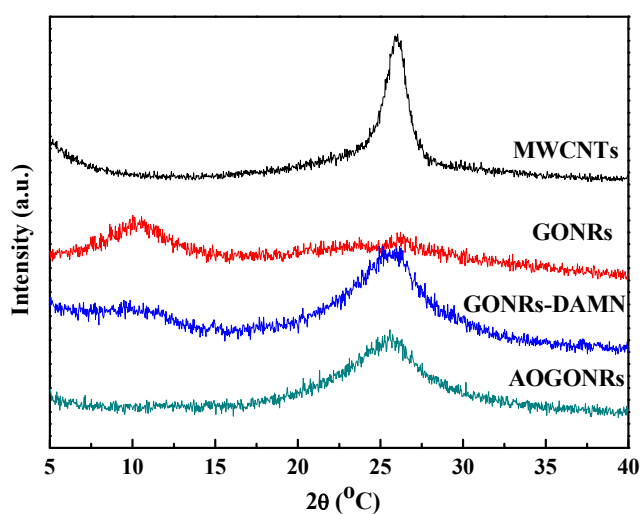


Fig. 3 XRD patterns of MWCNTs, GONRs, GONRs-DAMN and AOGONRs.

For the characterization of the major surface groups, FT-IR studies were carried out (Fig. 4). In the spectrum of MWCNTs, the bands at 3440 and 2920 cm^{-1} can be assigned to the O-H stretching vibration arising from the surface hydroxyl groups and saturated C-H vibration, respectively. The peak at 1578 cm^{-1} results from stretching vibrations of isolated C=C double bands and is partly superposed by a relatively strong water band at about 1634 cm^{-1} originating from residual humidity in the pellet.³² Compared to that of MWCNTs, a new peak of GONRs appears at 1714 cm^{-1} , which corresponds to the stretch of carboxylic (-COOH) groups.^{5,7} In the spectrum of GONRs-DAMN, the intensity of the 1714 cm^{-1} band (C=O) decreases sharply, and two new frequencies appear at 1468 cm^{-1} and 2206 cm^{-1} , separately, belonging to C-N and C \equiv N stretching vibrations, clearly supporting the presence of DAMN.²⁴ In the spectrum of AOGONRs, absorption band of cyano group at 2206 cm^{-1} disappeared while a new band at 942 cm^{-1} corresponding to N-O stretching vibrations of amidoxime groups was observed, indicating the consumption of cyano groups and the formation of the oxime groups after amidoximation.^{22,25}

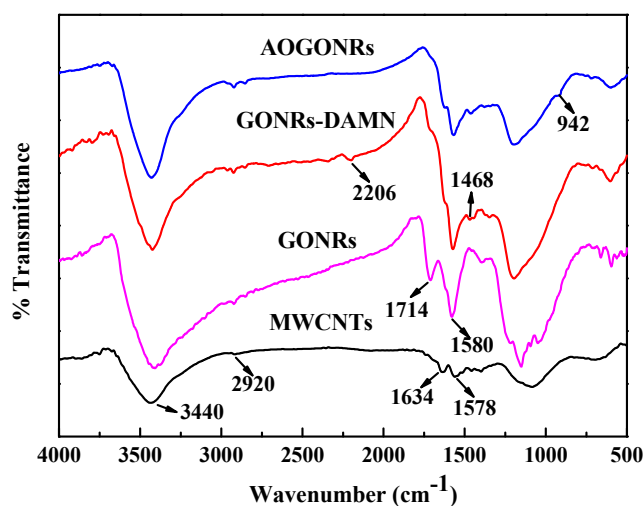


Fig. 4 FT-IR spectra of MWCNTs, GONRs, GONRs-DAMN and AOGONRs.

To further confirm the existence of cyano group and amidoxime groups, elemental analysis was measured and the results were shown in Table 2. Only a little nitrogen is detected in the GONRs, which could be ascribed to N-containing impurities. An obvious increase of nitrogen content was observed for GONRs-DAMN, indicating

that DAMN were grafted onto the surface of GONRs, as supported by the previous FT-IR analysis. The amounts of DAMN are calculated from the increment of the content of nitrogen to be about 3.11 mmol g^{-1} . It is also found that the carbon content decreased with the increase of nitrogen content from GONRs-DAMN to AOGONRs, which might be attributed to the transformation of cyano groups to amidoxime groups by the treatment of hydroxylamine in an alkaline medium.²⁴

Table 2 Elemental analysis of MWCNTs, GONRs, GONRs-DAMN and AOGONRs.

Samples	C %	H %	N %
MWCNTs	98.92	1.03	0.00
GONRs	62.58	1.69	0.43
GONRs-DAMN	59.12	2.81	9.14
AOGONRs	48.27	3.23	9.53

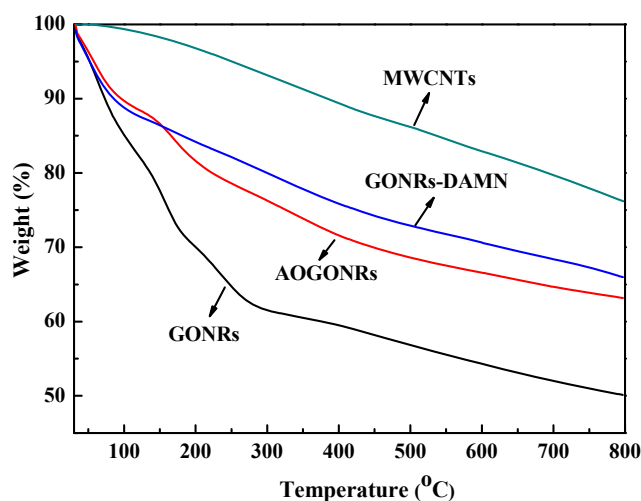


Fig. 5 TGA profiles of MWCNTs, GONRs, GONRs-DAMN and AOGONRs.

Fig. 5 shows the TGA curves of MWCNTs, GONRs, GONRs-DAMN and AOGONRs. The weight losses of the four materials can be divided into three main processes. The first stage ($\leq 150^\circ\text{C}$) can be attributed to the physically sorbed water possibly with residual solvent on the surface. In the second stage ($150 \sim 500^\circ\text{C}$), the weight losses of MWCNTs, GONRs, GONRs-DAMN and AOGONRs are 12.0%, 20.4%, 17.8%, 13.4%, respectively. For GONRs, it is attributed to the decomposition of the oxygen-containing functional groups. For GONRs-DAMN and AOGONRs, it is

owing to pyrolysis of the functional groups (mainly cyano groups and amidoxime group) covalently bound on the framework of the carbon-based nanomaterials.^{22, 33} The last stage (≥ 500 °C) is due to the release of CO₂ from the burning of carbon. The TGA profiles confirm that a significant amount of the functional groups have been exposed on the GONRs surface after grafting.

Effect of pH

The pH of aqueous solution is an important parameter for uranium(VI) sorption because it affects surface charge of the sorbent as well as the speciation of the solute. The effect of pH on uranyl ions sorption by AOGONRs was studied, and the results are shown in Fig. 6. The pH value investigated in this study was not higher than 4.5, because uranyl ions in the designed system would precipitate at higher pH values according to species distribution for U(VI) hydrolysis.²⁶

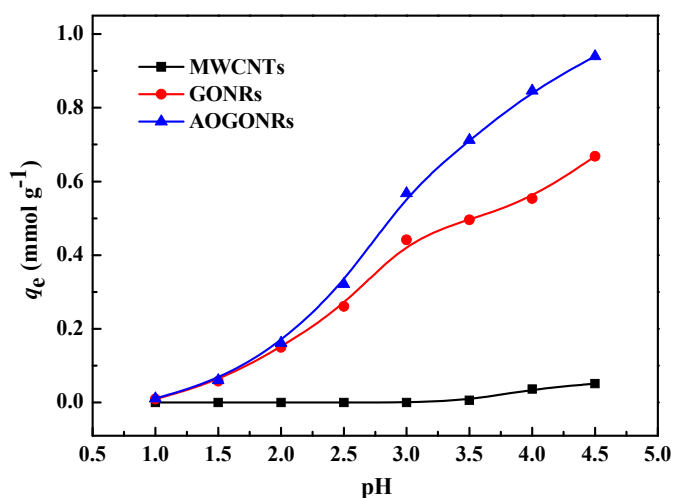


Fig. 6 Effect of pH on U(VI) sorption on MWCNTs, GONRs and AOGONRs, $w = 10$ mg, $C_0 = 0.25$ mmol L⁻¹, $t = 240$ min, $T = 298$ K, and $V = 50$ mL.

As can be seen from Fig. 6, the sorption amount of U(VI) on AOGONRs increases drastically with increasing pH, indicating that the sorption process is clearly pH-dependent. The low sorption at lower pH could be due to the protonation of oxime and imino group of amidoxime on AOGONRs and the competition of H⁺ with the active sites.³⁴ As the pH values increase, the protonation degree of the oxime groups

will be weakened and the hydroxyl proton in oxime group would be easily strip off,¹⁴ consequently favoring the sorption of UO_2^{2+} on AOGONRs. Furthermore, the sorption amount of U(VI) on AOGONRs is higher than that of MWCNTs and GONRs, implying that amidoximation of GONRs can improve the sorption capacity for U(VI).

Kinetic studies

Experiments were performed to study the effect of the contact time on U(VI) sorption on MWCNTs, GONRs and AOGONRs at different time varying from 2 to 120 min. As shown in Fig. 7, it is evident that the sorption amount of U(VI) on AOGONRs increased rapidly in the first 10 min, and the sorption equilibrium was reached within 20 min. However, the sorption amount of U(VI) on MWCNTs and GONRs increased slowly and the sorption equilibrium attained at 60 min. These observations showed that U(VI) sorption on AOGONRs was mainly through the surface complexation in a short reaction time.³⁵

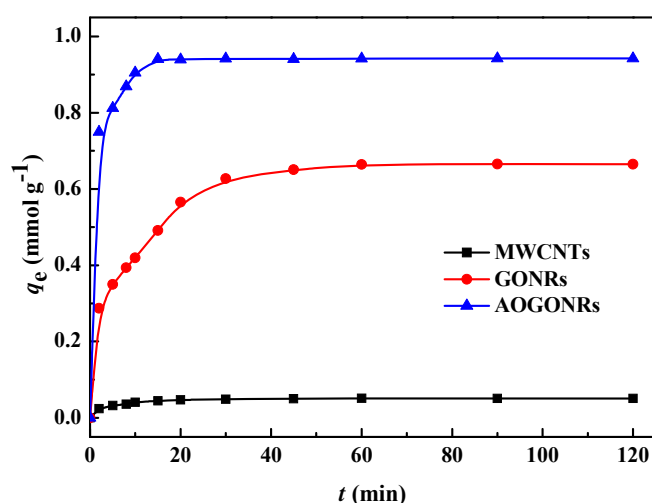


Fig. 7 Effect of contact time on the U(VI) sorption on MWCNTs, GONRs and AOGONRs, pH = 4.5, $w = 10$ mg, $C_0 = 0.25$ mmol L⁻¹, $T = 298$ K, and $V = 50$ mL.

Two different kinetic models, i.e. pseudo-first-order and pseudo-second-order were employed to describe the kinetic characteristic of U(VI) on three sorbents. The pseudo-first order kinetic model is expressed as the Eq. (3).

$$\ln(q_e - q_t) = \ln q_e - k_1 t \quad (3)$$

where q_e (mmol g^{-1}) and q_t (mmol g^{-1}) are the amounts of U(VI) adsorbed per gram of sorbent at equilibrium and at any time ' t ', respectively, k_1 (min^{-1}) is the sorption rate constants of pseudo-first-order.

The pseudo-second order kinetic model is always given as the Eq (4).

$$\frac{t}{q_t} = \frac{1}{k_2 q_e^2} + \frac{t}{q_e} \quad (4)$$

where k_2 ($\text{g mmol}^{-1} \text{min}^{-1}$) is the sorption rate constants of pseudo-first-order and pseudo-second-order sorption, respectively.

Table 3 The kinetic parameters of the U(VI) sorption onto MWCNTs, GONRs and AOGONRs.

Sorbents	q_e (mmol g^{-1})	Pseudo-first-order model			Pseudo-second-order model		
		k_1 (min^{-1})	$q_{e,\text{cal}}$ (mmol g^{-1})	R^2	k_2 ($\text{g mmol}^{-1} \text{min}^{-1}$)	$q_{e,\text{cal}}$ (mmol g^{-1})	R^2
MWCNTs	0.051	0.0557	0.0256	0.9716	7.41	0.052	0.9996
GONRs	0.668	0.0582	0.3191	0.9295	0.29	0.704	0.9987
AOGONRs	0.941	0.2048	0.3657	0.9388	2.02	0.948	0.9999

The sorption kinetic parameters in Eq. (3) and (4) were calculated from the slopes and intercepts of the plots of $\ln(q_e - q_t)$ versus t and t/q_t versus t , and the results were shown in Table 3. Obviously, The highest correlation coefficient value of pseudo-second-order model and the closest $q_{e,\text{cal}}$ to $q_{e,\text{exp}}$ indicated the pseudo-second-order model was more suitable to describe the sorption process of U(VI) on MWCNTs, GONRs and AOGONRs. The pseudo-second-order model was based on the assumption that the rate-determining step may be a chemisorption.³⁶

Sorption isotherms

The sorption isotherms of U(VI) on MWCNTs, GONRs and AOGONRs are presented in Fig. 8. It is obvious that AOGONRs have great enhancement on the sorption capacity of U(VI). A maximum sorption amount for U(VI) on AOGONRs was found to be about $2.112 \text{ mmol g}^{-1}$ (502.6 mg g^{-1}) at 298 K under this system, which is much higher than that of carbon-based nanomaterials as listed in Table 4.

Higher U(VI) sorption capacity of AOGONRs could be explained by chelating groups on AOGONRs groups. The presences of nitrogen- and oxygen-containing groups on the AOGONRs surface form complexes with uranyl species.^{17, 37} AOGONRs with such a high sorption ability to U(VI) exhibit a great potential of applications in removal and recovery of U(VI) from large volumes of aqueous solutions.

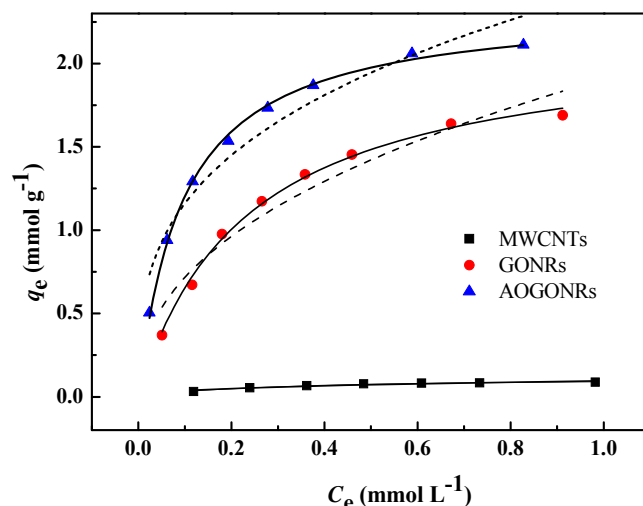


Fig. 8 Equilibrium isotherm for the U(VI) sorption on MWCNTs, GONRs and AOGONRs. The solid and dash lines represent the Langmuir and Freundlich model simulation, pH = 4.5, $w = 10$ mg, $t = 240$ min, $T = 298$ K, and $V = 50$ mL.

Table 4 Comparison of sorption capacity of U(VI) on various carbon-based nanomaterials.

Sorbents	Experimental conditions	Capacity (mg g^{-1})	Ref.
Pristine CNTs	pH = 5.0, r.t, I = 0.1 M NaClO ₄	4.28	32
CNTs treated with HNO ₃ and H ₂ SO ₄	pH = 5.0, r.t, I = 0.1 M NaClO ₄	45.9	32
Untreated MWCNTs	pH = 5.0, T = 308 K	39.5	38
Plasma functionalized MWCNTs	pH = 5.6, T = 293 K, I = 0.01 M NaClO ₄	17.35	39
Oxidized MWCNTs	pH = 5.0, T = 298 K, I = 0.01 M NaClO ₄	33.32	40
MWCNTs grafted with chitosan	pH = 5.0, T = 293 K, I = 0.01 M NaClO ₄	34.55	41
MWCNTs grafted with CMC	pH = 5.0, T = 298 K, I = 0.01 M NaClO ₄	111.9	28
Graphene oxide nanosheets	pH = 5.0, T = 293 K, I = 0.01 M NaClO ₄	97.5	5
Graphene oxide nanosheets	pH = 4.0, r.t	299	7
Reduced graphene oxide nanosheets	pH = 4.0, r.t	47	7
Magnetic graphene/iron oxides	pH = 5.5, T = 293 K, I = 0.01 M NaClO ₄	69.49	42
Amidoximated magnetite/graphene oxide composites	pH = 5.0, T = 298 K, I = 0.01 M NaClO ₄	284.9	25
Graphene oxide-activated carbon	pH = 5.5, T = 298 K	298	43
Graphene oxide nanosheets	pH = 4.0, T = 303 K, I = 0.01 M NaClO ₄	208.3	44
AOGONRs	pH = 4.5, T = 298 K, I = 0.01 M NaClO ₄	502.6	This work

Furthermore, experimental data were evaluated by both Langmuir isotherm and Freundlich isotherm models. The Langmuir isotherm model assumes that the sorption occurred on homogeneous surface by monolayer sorption. It can be expressed as

$$q_e = \frac{bq_m C_e}{1 + bC_e} \quad (5)$$

where q_m (mmol g^{-1}) and b (L mmol^{-1}) are the measure of Langmuir monolayer sorption capacity and the equilibrium constant related to the enthalpy of sorption, respectively.

The Freundlich model is usually appropriate to describe heterogeneous systems in the following equation:

$$q_e = K_F C_e^{1/n} \quad (6)$$

where K_F [$(\text{mmol g}^{-1}) (\text{L mmol}^{-1})^{1/n}$] and n are the Freundlich constants related to sorption capacity and the intensity of sorption, respectively.

The relative parameters calculated from the two models were listed in Table 5. The experimental data fit the Langmuir model better than the Freundlich one, suggesting that U(VI) absorbed on the surface form a monolayer coverage and chemisorption is the predominant mechanism.

Table 5 The parameters for the Langmuir and Freundlich isotherm models of U(VI) sorption on MWCNTs, GONRs and AOGONRs.

Sorbents	Langmuir			Freundlich		
	q_m (mmol g^{-1})	b (L mmol^{-1})	R^2	K_F [(mmol g^{-1}) ($\text{L mmol}^{-1})^{1/n}$]	n	R^2
MWCNTs	0.117	3.579	0.9795	0.0954	2.452	0.9030
GONRs	1.917	4.307	0.9947	1.9072	2.158	0.9337
AOGONRs	2.353	10.465	0.9976	2.4286	3.119	0.9343

Thermodynamic studies

The effect of temperature on U(VI) sorption on MWCNTs, GONRs and AOGONRs is also given in Fig. 9. The sorption amount of U(VI) increases gradually with the increase of temperature, which suggested that higher temperature was

beneficial to the U(VI) sorption process.

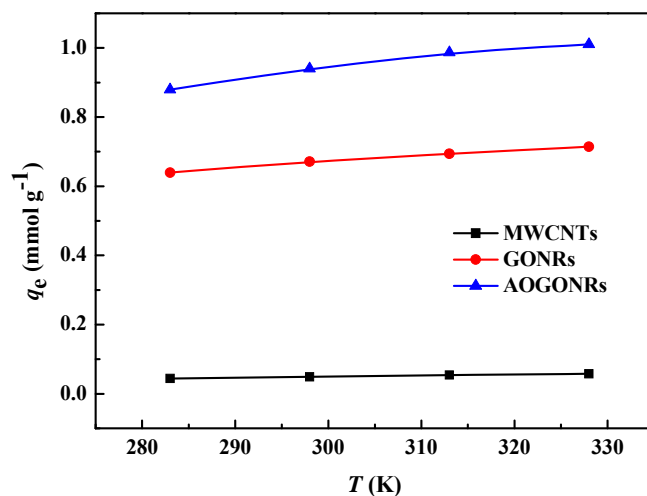


Fig. 9 Effect of temperature on the U(VI) sorption on MWCNTs, GONRs and AOGONRs, pH = 4.5, $w = 10$ mg, $C_0 = 0.25$ mmol L⁻¹, $t = 240$ min and $V = 50$ mL.

The temperature dependence of sorption process is associated with changes in several thermodynamic parameters such as stand free energy (ΔG), enthalpy (ΔH) and entropy (ΔS), which are calculated using the following Eq. (7) ~ (8) :

$$\ln K_d = \frac{\Delta S}{R} - \frac{\Delta H}{RT} \quad (7)$$

$$\Delta G = \Delta H - T\Delta S \quad (8)$$

where K_d is the distribution coefficient (mL g⁻¹), T and R are the absolute temperature (K) and the gas constant (8.314 J mol⁻¹ K⁻¹), respectively.

The values of ΔH and ΔS listed in Table 6 were calculated from the slope and intercept of the plots of $\ln K_d$ versus T^{-1} , and the values of ΔG were obtained using Eq. (8). The positive value of ΔH shows the endothermic nature of the sorption process on three sorbents. The positive value of ΔS suggests the increased randomness at the solid-liquid interface during the sorption on MWCNTs, GONRs and AOGONRs. The negative value of ΔG indicates that the adsorption reaction is spontaneous. In addition, the values of ΔG for MWCNTs, GONRs and AOGONRs at 298 K were -11.47, -19.73 and -22.10 kJ mol⁻¹, which indicated the sorption of U(VI) on AOGONRs was more favorable than MWCNTs and GONRs.

Table 6 Thermodynamic parameters for the U(VI) sorption on MWCNTs, GONRs and AOGONRs.

Sorbents	ΔH (kJ mol ⁻¹)	ΔS (J mol ⁻¹ K ⁻¹)	ΔG (kJ mol ⁻¹)			
			283 (K)	298 (K)	313 (K)	328 (K)
MWCNTs	4.82	54.69	-10.65	-11.47	-12.30	-13.12
GONRs	4.14	80.11	-18.53	-19.73	-20.93	-22.14
AOGONGs	9.99	107.72	-20.49	-22.10	-23.72	-25.34

Effect of ionic strength

The effect of ionic strength on the sorption capacity of AOGONRs for U(VI) at different NaNO₃ concentration (0-5.0 mol L⁻¹) was investigated. As shown in Fig. 10, the influence of U(VI) sorption on AOGONRs is considerably negligible, which further confirmed the higher affinity of AOGONRs toward U(VI). The characteristics of the as-synthesized sorbent could be favorable for use in certain key steps in any future sustainable nuclear fuel cycle.

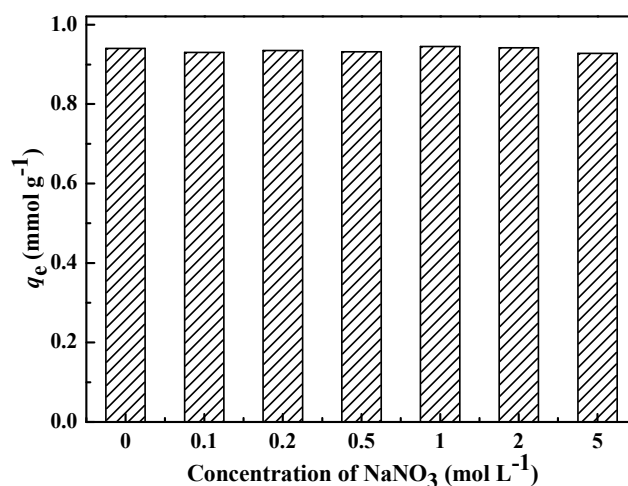


Fig. 10 Effect of ionic strength on U(VI) on AOGONRs, pH = 4.5, $w = 10$ mg, $C_0 = 0.25$ mmol L⁻¹, $t = 240$ min, $T = 298$ K and $V = 50$ mL.

Effect of competitive ions

To evaluate the sorption selectivity of both GONRs and AOGONRs, the effect of competitive cations was investigated in a simulated nuclear industrial effluent with 12 main sensible nuclides including uranyl ions. As shown in Fig. 11a, it is obviously

noticeable that the chemical modification has brought a distinct increase in U(VI) sorption capacity. The total sorption capacity of AOGONRs for all cations reached 2.27 mmol g⁻¹, which was much higher than that of GONRs (1.46 mmol g⁻¹). Meanwhile, the sorption capacity for U(VI) increased from 0.41 mmol g⁻¹ for GONRs to 1.35 mmol g⁻¹ for AOGONRs accounting for about 59.4% of the total sorption amount, which indicated that AOGONRs had markedly higher affinity to U(VI) ions. On the other hand, this selectivity can be further clarified by distribution coefficients (K_d). As shown in Fig. 11b, the K_d of AOGONRs reached high up to nearly 6000 mL g⁻¹ for U(VI) and lower (< 500 mL g⁻¹) for other coexistent ions, which suggested that amidoxime-functionalized GONRs exhibited a desirable selectivity for U(VI) ions over a range of competing metal ions.

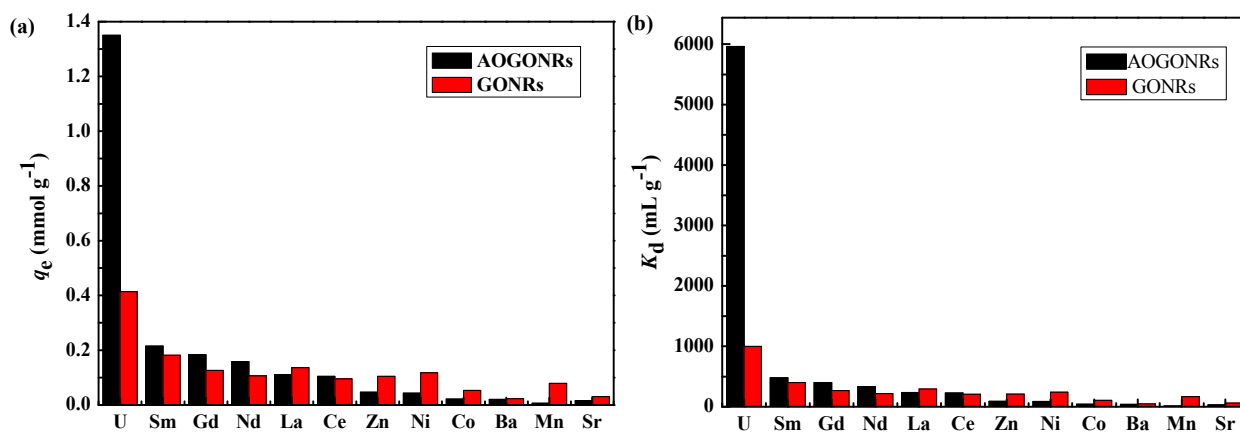


Fig. 11 (a) Competitive sorption capacities; (b) the K_d of coexistent ions of U(VI) on GONRs and AOGONRs, $C_0 = 0.5 \text{ mmol L}^{-1}$ for all cations, $\text{pH} = 4.5$, $t = 240 \text{ min}$, $w/V = 0.2 \text{ g L}^{-1}$, $T = 298 \text{ K}$.

Sorption mechanism

In order to further investigate the interaction mechanism between U(VI) and AOGONRs at a molecular level, XPS scans for AOGONRs before and after U(VI) sorption (denoted as AOGONRs-U(VI)) were measured. As shown in Fig. 12a, the peaks of C 1s, O1s and N1s are seen for the expected components of AOGONRs, and U 4f level is also detected, suggesting that uranium is adsorbed onto the surface of AOGONRs. Fig. 12b shows the presence of the characteristic doublets of U 4f_{5/2} and

U 4f_{7/2} at 393.0 and 382.3 eV with a splitting of about 10.7 eV.^{23, 45} The U 4f spectrum can be resolved into two peaks: the peak at 382.9 eV is assigned to the free uranyl adsorbed on AOGONRs, and the peak at 382.0 eV is attributed to a covalent bond of AO-U(VI).^{30, 46}

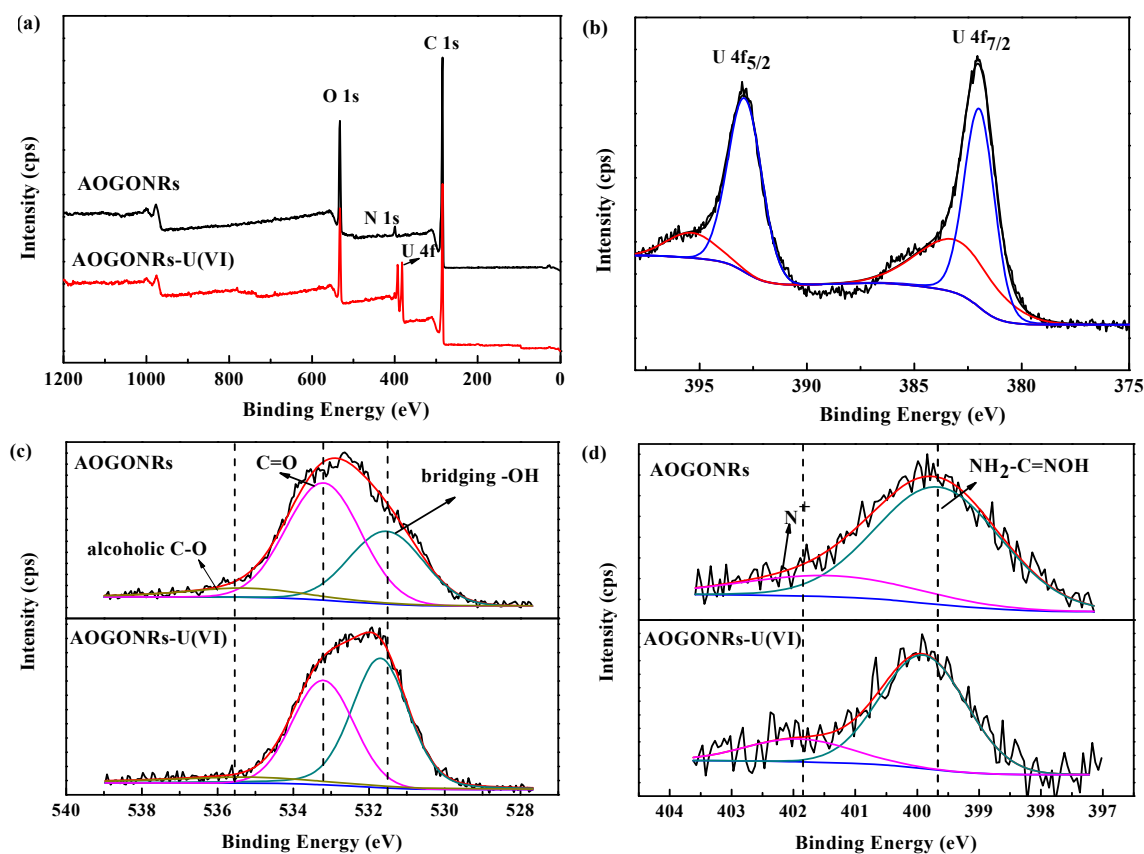


Fig. 12 (a) The typical XPS survey spectra of AOGONRs and AOGONRs-U(VI). High resolution XPS spectra of (b) U 4f, (c) O 1s and (d) N 1s.

The observed spectra of O 1s and N 1s of AOGONRs and AOGONRs-U(VI) were simulated using two-component Gaussian-Lorentzian sum functions. Fig. 12c shows the O 1s spectra of AOGONRs before and after U(VI) sorption. For the AOGONRs, it can be decomposed into three peaks at 531.5, 533.2 and 535.3 eV, which can be assigned to bridging -OH, C=O and alcoholic C-O, respectively.³⁰ Compared to AOGONRs, a higher binding energy of the bridging -OH peak is observed and the relative intensities of the C=O and C-O peaks of AOGONRs-U(VI) decrease. The great variation of O 1s before and after U(VI) sorption indicates that UO_2^{2+} can form

strong complexes with oxygen-containing functional groups.

As shown in Fig. 12d, the N 1s spectrum in AOGONRs composites could be separated into two peaks: the peak at 399.6 eV corresponds to $\text{NH}_2\text{-C=NOH}$, and the peak at 401.5 eV is related to cationic nitrogen atoms (N^+).⁴⁷ Compared to AOGONRs, the position of $\text{NH}_2\text{-C=NOH}$ after U(VI) sorption was shifted to higher binding energy. This change could be ascribed to the formation of the complexes between $\text{NH}_2\text{-C=NOH}$ and UO_2^{2+} , in which UO_2^{2+} shares electrons with the nitrogen atom in amidoxime group.^{48, 49}

Based on analysis of the XPS spectra and previous sorption behavior, the high sorption ability of AOGONRs is largely due to large number of nitrogen- and oxygen-containing functional groups in amidoxime groups, which can easily form strong complexes with UO_2^{2+} on the AOGONRs surface.

Desorption and reusability studies

The repeated availability is also very important for the practical application when evaluating the economy and applicability of sorbents. In this work, the desorption experiments of U(VI) was performed with HCl solutions in the concentration range from 0.1 to 2.0 mol L⁻¹. As shown in Fig. 13, about 98% of U(VI) ions can be desorbed using 0.5 mol L⁻¹ HCl. Consequently, 0.5 mol L⁻¹ HCl aqueous solution was selected as desorbing agent for AOGONRs.

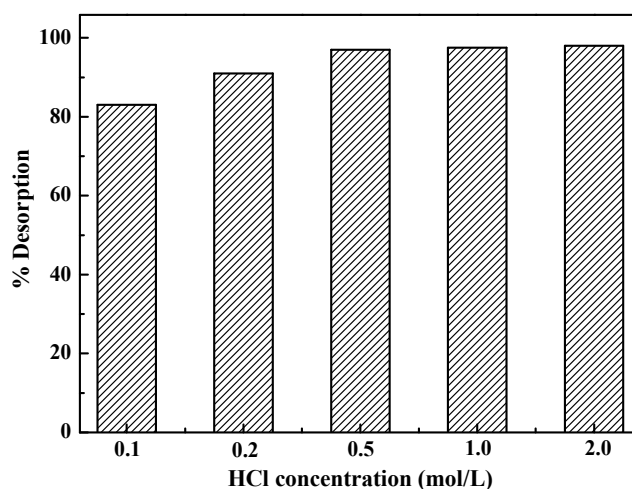


Fig. 13 Effect of HCl concentration on U(VI) desorption.

To assess the reusability of sorbent, regenerated AOGONRs was used for five consecutive sorption/desorption cycles. As shown in Fig. 14, the sorption amount of U(VI) decreased slightly from 0.94 mmol g⁻¹ to 0.89 mmol g⁻¹ after five consecutive cycles, indicating that AOGONRs present excellent reusability and can be used as a good sorbent applied in the field of U(VI) removal and recovery.

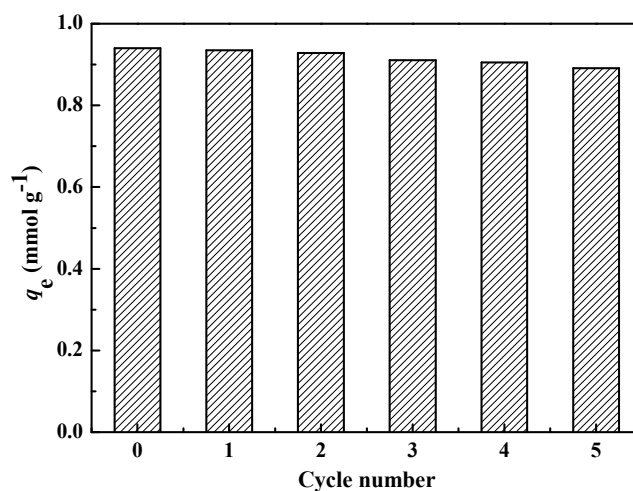


Fig. 14 Regenerated use of AOGONRs, pH = 4.5, $w = 10$ mg, $C_0 = 0.25$ mmol L⁻¹, $t = 240$ min, and $T = 298$ K.

Conclusions

Amidoxime-functionalized GONRs sorbent was successfully synthesized in the present work. The raw materials MWCNTs for GONRs are commercially available and cheaper than graphene. AOGONRs have not only strong affinity but also high selectivity toward uranium(VI) even in multi-ion system and test solution with weak acidity and high ionic strength. Uranium sorption on AOGONRs was pH-dependent, ionic strength-independent, fast, endothermic, spontaneous and a pseudo-second order process. Repeated sorption-desorption experiments indicated AOGONRs can be effectively regenerated and reused for U(VI) sorption without obvious loss in the sorption amount. The results suggested that the new GONRs-based sorbent may be a promising candidate for application in selective separation of uranium from nuclear fuel effluents as well as other related water sources.

Acknowledgement

This work was supported by the National Natural Science Foundation of China (Grants No. 91226108), NASF (Grants No. U1330125), the Ph.D. Programs Foundation of Ministry of Education of China (Grants No. 20110181120001), and the National Fund of China for Fostering Talents in Basic Science (J1210004).

References

1. A. K. Geim and K. S. Novoselov, *Nature Materials*, 2007, **6**, 183-191.
2. H. Chang and H. Wu, *Energy & Environmental Science*, 2013, **6**, 3483-3507.
3. D. K. James and J. M. Tour, *Accounts of Chemical Research*, 2012, **46**, 2307-2318.
4. L. Tan, Y. Wang, Q. Liu, J. Wang, X. Jing, L. Liu, J. Liu and D. Song, *Chemical Engineering Journal*, 2015, **259**, 752-760.
5. G. Zhao, T. Wen, X. Yang, S. Yang, J. Liao, J. Hu, D. Shao and X. Wang, *Dalton Transactions*, 2012, **41**, 6182-6188.
6. A. Y. Romanchuk, A. S. Slesarev, S. N. Kalmykov, D. V. Kosynkin and J. M. Tour, *Physical Chemistry Chemical Physics*, 2013, **15**, 2321-2327.
7. Z. Li, F. Chen, L. Yuan, Y. Liu, Y. Zhao, Z. Chai and W. Shi, *Chemical Engineering Journal*, 2012, **210**, 539-546.
8. N. Pan, D. Guan, T. He, R. Wang, I. Wyman, Y. Jin and C. Xia, *Journal of Radioanalytical and Nuclear Chemistry*, 2013, **298**, 1999-2008.
9. Y. Sun, Q. Wang, C. Chen, X. Tan and X. Wang, *Environmental Science & Technology*, 2012, **46**, 6020-6027.
10. L. Ma, J. Wang and F. Ding, *ChemPhysChem*, 2013, **14**, 47-54.
11. A. Hirsch, *Angewandte Chemie International Edition*, 2009, **48**, 6594-6596.
12. D. V. Kosynkin, A. L. Higginbotham, A. Sinitskii, J. R. Lomeda, A. Dimiev, B. K. Price and J. M. Tour, *Nature*, 2009, **458**, 872-876.
13. Y. Wang, Z. Wang, Z. Gu, J. Yang, J. Liao, Y. Yang, N. Liu and J. Tang, *Journal of Radioanalytical and Nuclear Chemistry*, 2015, **304**, 1329-1337.
14. Y. Zhao, J. Li, L. Zhao, S. Zhang, Y. Huang, X. Wu and X. Wang, *Chemical Engineering Journal*, 2014, **235**, 275-283.

15. C.-Z. Wang, J.-H. Lan, Q.-Y. Wu, Q. Luo, Y.-L. Zhao, X.-K. Wang, Z.-F. Chai and W.-Q. Shi, *Inorganic chemistry*, 2014, **53**, 9466-9476.
16. X. Liu, H. Liu, H. Ma, C. Cao, M. Yu, Z. Wang, B. Deng, M. Wang and J. Li, *Industrial & Engineering Chemistry Research*, 2012, **51**, 15089-15095.
17. N. Horzum, T. Shahwan, O. Parlak and M. M. Demir, *Chemical Engineering Journal*, 2012, **213**, 41-49.
18. Y. Yue, X. Sun, R. T. Mayes, J. Kim, P. F. Fulvio, Z. Qiao, S. Brown, C. Tsouris, Y. Oyola and S. Dai, *Science China Chemistry*, 2013, **56**, 1510-1515.
19. J. Górká, R. T. Mayes, L. Baggetto, G. M. Veith and S. Dai, *Journal of Materials Chemistry A*, 2013, **1**, 3016.
20. M. Carboni, C. W. Abney, K. M. L. Taylor-Pashow, J. L. Vivero-Escoto and W. Lin, *Industrial & Engineering Chemistry Research*, 2013, **52**, 15187-15197.
21. D. Shao, J. Li and X. Wang, *Science China Chemistry*, 2014, 1-10.
22. X. Yang, J. Li, J. Liu, Y. Tian, B. Li, K. Cao, S. Liu, M. Hou, S. Li and L. Ma, *Journal of Materials Chemistry A*, 2014, **2**, 1550.
23. A. Gopalan, M. F. Philips, J.-H. Jeong and K.-P. Lee, *Journal of Nanoscience and Nanotechnology*, 2014, **14**, 2451-2458.
24. J. Geng, L. Ma, H. Wang, J. Liu, C. Bai, Q. Song, J. Li, M. Hou and S. Li, *Journal of Nanoscience and Nanotechnology*, 2012, **12**, 7354-7363.
25. Y. Zhao, J. Li, S. Zhang, H. Chen and D. Shao, *RSC Advances*, 2013, **3**, 18952.
26. Y. Wang, Z. Gu, J. Yang, J. Liao, Y. Yang, N. Liu and J. Tang, *Applied Surface Science*, 2014, **320**, 10-20.
27. A. L. Higginbotham, D. V. Kosynkin, A. Sinitskii, Z. Sun and J. M. Tour, *ACS Nano*, 2010, **4**, 2059-2069.
28. D. Shao, Z. Jiang, X. Wang, J. Li and Y. Meng, *The Journal of Physical Chemistry B*, 2009, **113**, 860-864.
29. J. Wang, Z. Shi, Y. Ge, Y. Wang, J. Fan and J. Yin, *Journal of Materials Chemistry*, 2012, **22**, 17663-17670.
30. W. Song, X. Wang, Q. Wang, D. Shao and X. Wang, *Physical Chemistry Chemical Physics*, 2015, **17**, 398-406.

31. Y. Wang, Z. Shi and J. Yin, *The Journal of Physical Chemistry C*, 2010, **114**, 19621-19628.
32. A. Schierz and H. Zanker, *Environmental pollution*, 2009, **157**, 1088-1094.
33. S. M. Badawy, H. H. Sokker, S. H. Othman and A. Hashem, *Radiation Physics and Chemistry*, 2005, **73**, 125-130.
34. K. Singh, C. Shah, C. Dwivedi, M. Kumar and P. N. Bajaj, *Journal of Applied Polymer Science*, 2013, **127**, 410-419.
35. Y. Sun, C. Ding, W. Cheng and X. Wang, *Journal of Hazardous Materials*, 2014, **280**, 399-408.
36. B. Li, L. Ma, Y. Tian, X. Yang, J. Li, C. Bai, X. Yang, S. Zhang, S. Li and Y. Jin, *Journal of Hazardous Materials*, 2014, **271**, 41-49.
37. S. P. Dubey, A. D. Dwivedi, M. Sillanpää, Y.-N. Kwon and C. Lee, *RSC Advances*, 2014, **4**, 46114-46121.
38. I. I. Fasfous and J. N. Dawoud, *Applied Surface Science*, 2012, **259**, 433-440.
39. M. Song, Q. Wang and Y. Meng, *Journal of Radioanalytical and Nuclear Chemistry*, 2012, **293**, 899-906.
40. Y. Sun, S. Yang, G. Sheng, Z. Guo and X. Wang, *Journal of environmental radioactivity*, 2012, **105**, 40-47.
41. D. Shao, J. Hu and X. Wang, *Plasma Processes and Polymers*, 2010, **7**, 977-985.
42. P. Zong, S. Wang, Y. Zhao, H. Wang, H. Pan and C. He, *Chemical Engineering Journal*, 2013, **220**, 45-52.
43. S. Chen, J. Hong, H. Yang and J. Yang, *Journal of environmental radioactivity*, 2013, **126**, 253-258.
44. C. Ding, W. Cheng, Y. Sun and X. Wang, *Dalton Transactions*, 2014, **43**, 3888-3896.
45. D. Shao, G. Hou, J. Li, T. Wen, X. Ren and X. Wang, *Chemical Engineering Journal*, 2014, **255**, 604-612.
46. X. Wang, S. Zhang, J. Li, J. Xu and X. Wang, *Inorganic Chemistry Frontiers*, 2014, **1**, 641-648.
47. H. Chen, D. Shao, J. Li, A. Alsaedi and X. Wang, *Chemical Engineering Journal*, 2014, **255**, 604-612.

- 2014, **254**,623-634.
48. W. Song, M. Liu, R. Hu, X. Tan and J. Li, *Chemical Engineering Journal*, 2014, **246**, 268-276.
49. Z. Yu, E. Kang and K. Neoh, *Langmuir*, 2002, **18**, 10221-10230.